OPTIGRID

D2.2 - Meteorological forecast data - Coupling NWP and CFD Modeling. Merging the datasets

September 2021

Project Name:	Document Number:	Revision:	Date:
OPTIGRID	D2.2	v1	2021-09-30
Funding:	Authors:	Reviewed by:	Approved by:
PTDC/EEI-EEE/31711/2017*	António Couto	Joaquim Duque	Rui Pestana
	Acknowledgements:		
	Frederico Melo		

*Project PTDC/EEI-EEE/31711/2017 submitted under the call for tenders (AAC) No. 02 / SAICT / 2017, and funded by national funds through the budget of the Foundation for Science and Technology (FCT).

Executive Summary

The work presented in this deliverable was developed by LNEG and R&D NESTER as part of the R&D activities of the project *OPTIGRID - Methodology for the dynamic line rating analysis and optimal management of power networks*. According to the plan activities of Tasks 2.1 and 2.4, the main objective of this deliverable is to present the methods applied to obtain the meteorological forecast data need to feed the models developed in this project and it merges all the datasets to be used in each case study.

According to the work plan, and as reported in the deliverables from Task 4, three case studies were defined for: A) a region with large distributed wind capacity; B) a region with large photovoltaic (PV) potential and limited grid capacity; and C) market splitting occurrence in MIBEL due to congestion in the interconnections. For these regions the meteorological forecast data, used during this project, were obtained using a numerical weather prediction model and computational fluid dynamic model coupling approach. The numerical weather prediction (NWP) model is used to forecast the hourly spatial meteorological data (e.g., wind speed and direction, temperature) during 2018 with a maximum spatial resolution of 3 km. This model is calibrated regarding its physical parametrizations and initial/boundary conditions, among others.

For case studies A and B, a physical downscaling of the NWP data was implemented using a CFD model with a one-way nesting approach. The CFD simulations are performed using high-resolution terrain and roughness data to capture local scale effects on the meteorological parameters with the highest impact on the determination of the capacity factor of the overhead electric lines – wind speed and direction. For the C case study, due to the extension of the regions under analysed, it was used only data extracted from the NWP model.

The meteorological and the transmission network data were gathered for 2018 using one-hour time resolution. A common coordinate reference system was established for the georeferenced data, and all the temporal data were carefully analysed and synchronized.

Within the scope of this project, all the data needed for the development of the mathematical models were made available and used. However, for confidentiality reasons, only non-confidential data are presented in this report.

Table of Contents

List of Figures

List of Tables

1. Introduction

The present deliverable was developed by the Laboratório Nacional de Energia e Geologia (LNEG) and R&D NESTER as part of the R&D activities of the OptiGRID project - *Task 2: Meteorological, network and market data* - that deal with the data gathering and validation for the research activities foreseen in this project. This report specifically describes the approach implemented to obtain the relevant meteorological data that will feed the methodology under development in this project for the dynamic line rating (DLR) analysis and optimal management of power networks.

The DLR typical approaches can be split into two main groups: *i)* direct monitoring of the conductor's physical parameters (*e.g.*, line temperature and sag monitoring), and *ii)* indirect monitoring through the meteorological environmental parameters (*e.g.*, wind speed and direction) that affect line rating assessment [1]. The benefits of the different approaches, as well as their application to different case studies, are discussed in [2], [3]. While the first one can be considered more accurate compared to the indirect approach, this approach, based on local sensors measuring the power line characteristics, raises some challenges. One of the main challenges is the significant capital and operational expenditures of such equipment to cover enough points of a network.

In the indirect approach, this challenge can be easily overcome by using numerical weather prediction (NWP) models. This type of model has been used in the latest years in the energy sector to obtain reliable time series of meteorological parameters (e.g. wind speed and direction) representative of a region, without the installation of an extensive and costly network of meteorological stations [4]. NWP models enable describing the behaviour and evolution of the air masses and explicitly treat the atmospheric phenomena down to a spatial resolution of 1x1 km.

Despite improvements in NWP, systematic phase and amplitude errors, in the low levels of the atmosphere, are unavoidable due to, e.g., the inability of these models to handle successfully the so-called local effects originated by roughness and orography. To properly account for these local effects on the flow, statistic or physical downscaling techniques of the NWP model outputs can be applied to correct the data providing location-specific forecasts [5], [6]. The statistical approach needs a considerable number of meteorological stations [5]. In the physical approach, the use of microscale models, namely, the computational fluid dynamic (CFD) models widely accepted in the energy industry, requires only a reduced number of stations (observed or virtual[1]). Although with different configurations, the NWP-CFD coupling was already implemented by several authors that highlight the models' complementarity in solving different spatial and temporal phenomena [7], [8]. Thus, the coupling of NWP and CFD models can represent a techno-economic solution to implement in real-time the DLR analysis of overhead power lines for a region of control. This deliverable proposes and implements an NWP-CFD approach considering its application in real-time operation.

To easily handle all the data gathered in Task 2 a single dataset was created. For this purpose, a common coordinate reference system was established for the georeferenced data. For the time-series data, a set of algorithms were implemented to allow i) rigorous quality control procedures of all temporal data available, and ii) synchronization of the data.

[1] Virtual time series [16] refers to site-specific time series of meteorological parameters retrieved from numerical models.

2. Literature review

2.1 Influence of meteorological parameters on conductor temperature

The influence of meteorological parameters on conductor temperature can change due to the non-linear nature of heat transfer mechanisms. Consequently, the ampacity that can be unlocked by considering the influence of meteorological parameters to calculate the capacity of overhead lines is very important and has been the subject of several works.

The role of meteorological conditions in the conductor thermal behaviour is discussed by several authors [9], [10]. The wind speed is described as the parameter with the greatest impact in the cooling of lines, followed by wind direction and ambient temperature, while the effect of solar radiation is much reduced when compared with the previous parameters, as mentioned by several authors, e.g., [11]–[13]. Figure 1 shows the current intensity dependency of the different meteorological parameters. In this figure, only one parameter is changed and the remaining parameters are kept constant (see Annex A for further details). The values were computed using the CIGRÉ formulation [14].

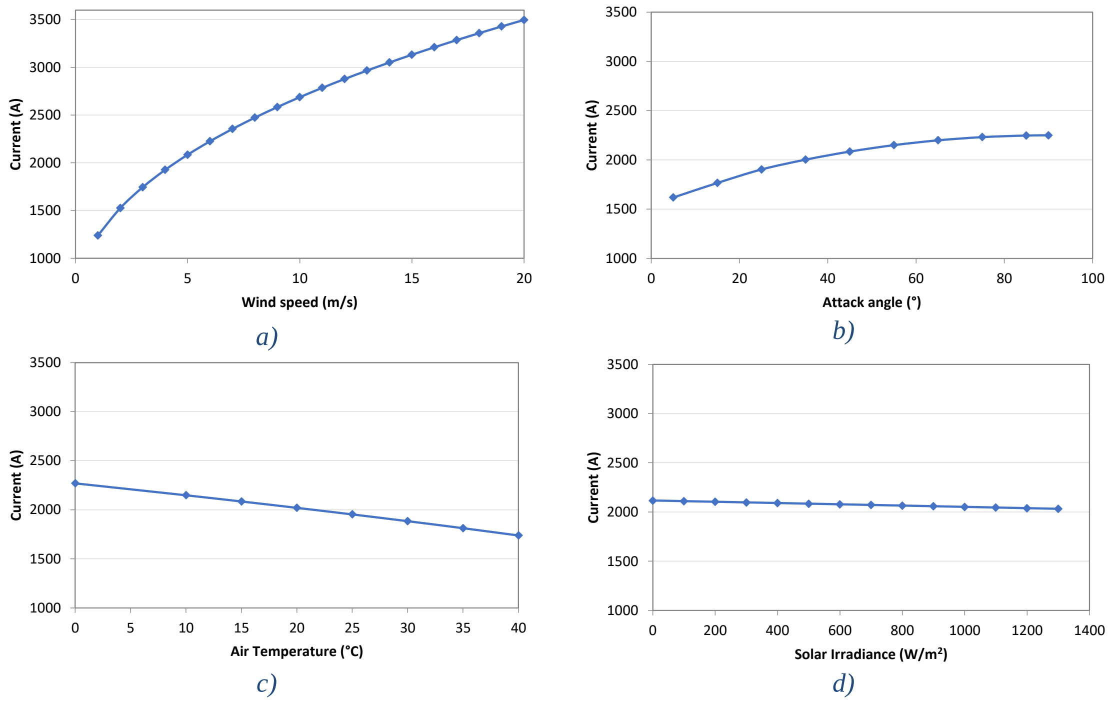

Figure 1 – Example of the impact of meteorological parameters in the DLR analysis of overhead power lines.

A closer inspection of Figure 1 highlights an approximately logarithmic behaviour between wind speed and the ampacity obtained. The wind speed has a very high spatial and temporal variability, showing variations in its magnitude along an overhead power line. Inside the planetary boundary layer, the wind speed and direction presents a great variability due to the influence of roughness, the terrain orography and obstacles. According to [13], [15], for reduced wind speeds, an high influence of the remaining parameters is expected, making them critical factors.

The cable's wind incident direction shows an influence smaller on the ampacity compared to the one observed in the wind speed. The maximum ampacity value is obtained for angles close to 90° (incident angle perpendicular to the cable), which is expected according to convection heat transfer theory [11].

The impact of temperature on the ampacity of conductors can be perceived in Figure 1c). Results suggest an approximately linear behaviour. According to [13], for the DLR analysis, a mean square error of less than 2ºC in the estimation of this meteorological parameter is quite satisfactory. Indeed, when compared with wind speed and direction, the ambient temperature has a low temporal and spatial variability in areas of less complex orography. In regions with very complex orography, it is essential to evaluate the temperature more precisely so as not to incur high errors in the application of DLR analysis.

The solar irradiance influence on the power lines' ampacity is reduced, remaining approximately constant. Nevertheless, as previously discussed, for reduced wind speed values (below 0.5 m/s), it can become an important and limiting parameter of the maximum permissible ampacity [11].

2.2 Wind speed and direction characterization

The assessment of the wind resource in a given region is a crucial step in managing the use of the wind resource as an energy source. Historically, the assessment of the wind resource on a regional and/or national scale was carried out through a few anemometric stations complemented with geostatistical methods (interpolations or semi-empirical correlations) leading to estimates with low precision and accuracy [16]. With the growing need to evaluate the wind resource for different applications, new models to increase the precision in the simulation of wind flow were developed. These models can be classified into linear and non-linear [17]. Linear models have the advantage of needing low computational resources and enabling the wind resource evaluation, with reasonable accuracy, for flat orography with small elevations, i.e., under non-complex terrain conditions. However, these models tend to miscalculate the wind speed behaviour in the lee-side of the hills [17]. Therefore, these models are unsuitable for complex terrain.

The advances in numerical modelling together with the increase in computational capabilities enabled the development of non-linear models in the flow simulation industry and the assessment of wind potential. Among these non-linear models, in the wind sector, computational fluid dynamics (CFD) models stand out enabling increased accuracy of the wind potential assessments, especially in complex terrain [18]. Results from several authors already highlighted the benefits of this model against the linear models [19]. Furthermore, the inclusion of thermal effects in the stratification in CFD simulations result in calculations with greater precision.

The use of mesoscale numerical models is one of the most common approaches to mitigating the costly installation and the anemometric stations maintenance costs for wind potential assessment. These models allow solving the differential equations that translate the physical laws describing the dynamic behaviour of the atmosphere, up to a maximum spatial resolution of 1x1 km, allowing to obtain the most relevant meteorological parameters for the characterization of the wind resource, e.g., wind intensity and direction [20]. These models can describe atmospheric phenomena such as the behaviour and propagation of air masses and explicitly address the inherent phenomena of atmospheric turbulence and stratification.

To increase the precision and accuracy of the results of the evaluation of the wind flow and tacking into account the spatiotemporal resolution capabilities inherent in the mesoscale and microscale models, it is possible to proceed to the so-called NWP-CFD models coupling. This method can be performed by coupling and nesting information in a unidirectional or bidirectional form between the different models and, specifically, in this work's microscale and mesoscale models. According to [18], the coupling method represents a robust methodology for evaluating the wind potential at any level within the atmospheric boundary layer. The accuracy of this methodology is significantly sensitive to the complexity of the terrain. Therefore, to reduce the corresponding errors, an adequate terrain discretization is crucial. In the same study, errors of close to 15% were obtained, both in the evaluation of the annual energy produced and in the average wind speed. According to [8], the use of coupling methods allowed an error reduction of approximately 50% compared to the use of only mesoscale models. Furthermore, it demonstrated that the greater the complexity of the terrain to be simulated, the greater the importance of coupling different models to capture the effects of orography on wind flow and, consequently, minimize errors in the estimation of atmospheric flow.

In [21] the author explores several NWP-CFD approaches and applied them to virtual overhead power lines based on the meteorological and anemometric stations from Perdigão experimental campaign[2]. The approaches include the use of virtual time series extracted for several heights and spatial points and also a nesting coupling of the initial and boundary conditions of the CFD model using the information from the mesoscale model. The author also addressed the dependence of the virtual series on the vertical plane. It is possible to conclude that among the heights evaluated (average height of the overhead power line, average height used in the wind sector, and average planetary boundary layer in the region under analysis). Using virtual time series, the highest performance was identified for the following conditions:

i) the geographic point that minimizes the difference in the height above ground elevation between the point of extraction of mesoscale data and the introduction point of the virtual series in the CFD model.

ii) 80 meters above the mean sea level. The results suggest that feeding the CFD model with virtual series for heights close to the ground or very far from it may not correspond to the best option for evaluating the wind speed and direction.

Finally, the authors point out the spatial terrain grid resolution of 30 meters presents better results when compared with high-resolution grids, in specific, 10 and 15 meters.

[2] More details regarding this experimental campaign available at: https://perdigao.fe.up.pt/

3. Methods

The main steps to obtain the meteorological data are presented in Figure 2. This approach was applied to case studies A and B. In the case study C, only data from the NWP were used.

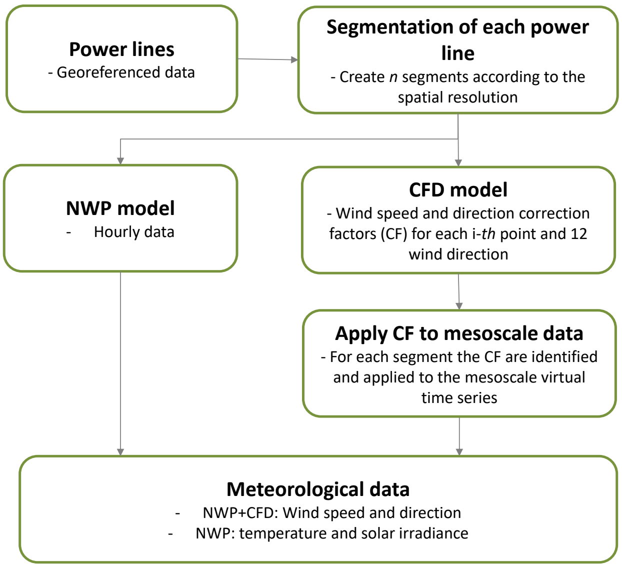

Figure 2 – Coupling approach implemented in the OptiGRID project.

The methodology implemented uses the information from the vertices towers to split the network lines into *n* segments according to the spatial resolution of the meteorological data. It is assumed that each line segment experiences the hourly meteorological conditions extracted for its central (mid-distance) point. The identification of the central point is pre-identified with the tool under development in OptiGRID project.

The hourly NWP data is extracted for this central point using an inverse distance weighted interpolation of the four neighbour's grid points in the case of air temperature and solar irradiance parameters. All the data are extracted to 25 meters above ground level. This height is a conservative value and it was estimated after analysing the average height of overhead lines spans of the conductors for several power lines in Portugal. Since it is used the same CFD model, for the wind speed and direction, it was decided to use the best NWP-CFD calibration identified in [21], which was described in section 2.2.

3.1 Mesoscale Model: MM5

The mesoscale model used in this work was the Fifth-generation model (aka MM5) [22]. The MM5 numerical model is an open-access mesoscale atmospheric model, which is being continuously improved through the contribution of various users from universities and research institutes around the world. Although the MM5 was originally developed for short-term weather forecasting, it has experienced many changes over the years making it suitable for simulating atmospheric conditions in the low levels of the atmosphere.

The optimal configuration of this type of model requires sensitivity tests to the most relevant features using observed data. According to [23] key features of these models are: initial and boundaries conditions (IBC) obtained through reanalysis/analysis projects, model's physical parameterizations, and data assimilation schemes. Regarding the IBC, operationally, the Global Forecast System (GFS) [24] is the most used database since it is publicly available. The global model GFS 0.25º simulates the dynamics of the troposphere/tropopause and part of the stratosphere at a spatial resolution of 0.25º × 0.25º (approximately 28 km ×28 km in the region under analysis in this work) using 31 vertical levels of the atmosphere – mandatory levels at standard altitudes for numerical weather and aeronautical forecasting purposes up to the altitude of 25km.

The physical parameterizations were selected taking into account the typical climatic characteristics over Portugal [25]. For the data assimilation, the most suitable scheme identified in [25] is also used. This scheme consists of the Four-Dimensional Data Assimilation (FDDA) method. Further details regarding the model configuration are presented in section 4.1.

3.1.1 Specification of the meteorological forecast data for the day-ahead market

Figure 3 depicts the time frame of interest for this project that focuses on the day-ahead market (DAM) from the Iberian electricity market (MIBEL). The current DAM design requires, at 12 noon on day *D*, the forecast of electricity production for the 24 hours on the next day (*D+1*) from all participating producers. On the other hand, updated IBC needed for the NWP are usually provided at 00, 06, 12, and 18 hours UTC of each day. In this case, the 06 UTC needs to be used, which corresponds to a time lag up to 18h between the meteorological data and the first hour of operation. Despite the recent improvements observed in the power forecasts systems, large errors are still observed, especially for long time horizons (that involve a time lag up to 42 hours in some cases) as the ones currently still required by electricity markets. Therefore, and since no experimental campaign was foreseen in this project the results obtained should be carefully analyzed.

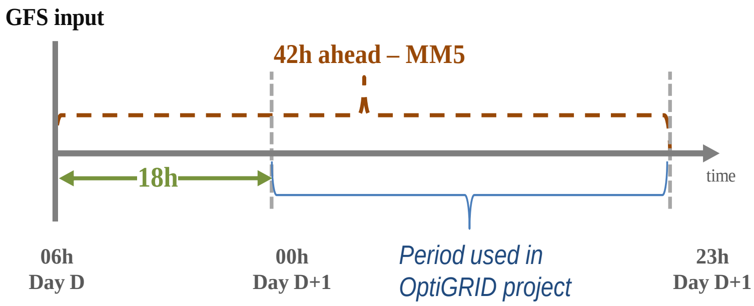

Figure 3 – Time frames for providing the NWP data.

3.2 CFD Model: WindSim

The CFD model used in this work is the WindSim software[3]. The main principles and capabilities of WindSim can be consulted in the literature [8], [19], [26]–[31]. This software uses the solution of Reynolds equations. That is, the equations are deduced from the Navier-Stokes equations using a time-averaging procedure [26]. Contrary to a step-by-step approach applied to linear models, the flow simulation starts by defining the theoretical boundary conditions by the user. Thus, applying a turbulence model, the equations are solved through an iterative process until the solution converges to a predefined convergence criterion [31]. The Navier-Stokes equations defined in the WindSim methodology are expressed in the form of a Cartesian tensor:

$$\frac{\partial U_i}{\partial x_i} = 0 \tag{1}$$

$$U_j \frac{\partial U_j}{\partial x_j} = -\frac{1}{\rho}\frac{\partial P}{\partial x_i} + \frac{\partial}{d x_j}\left(\upsilon\left(\frac{\partial U_i}{\partial x_j} + \frac{\partial U_j}{\partial x_i}\right) - \left(\overline{u_i u_j}\right)\right) \tag{2}$$

[3] Further details of the software are available at: https://windsim.com/

where U is the velocity, x is the spatial position, P is the atmospheric pressure, ρ corresponds to the air density, ν is the kinematic viscosity, and the subscripts i and j are unit direction vectors. Note that turbulence is obtained by relating the Reynolds stress number to the mean velocity through the turbulent viscosity:

$$\overline{u_i u_j} = \nu_T \left(\frac{\partial U_i}{\partial x_j} + \frac{\partial U_j}{\partial x_i} \right) + \frac{2}{3} \delta_{ij} k \tag{3}$$

where ν_T is the turbulent viscosity and k is the turbulent kinetic energy.

WindSim uses a modular structure consisting of six modules, as can be seen in Figure 4. The first three modules only run if the previous module is correctly simulated. The remaining three modules run independently of each other, but with the condition that the three initial modules are executed beforehand.

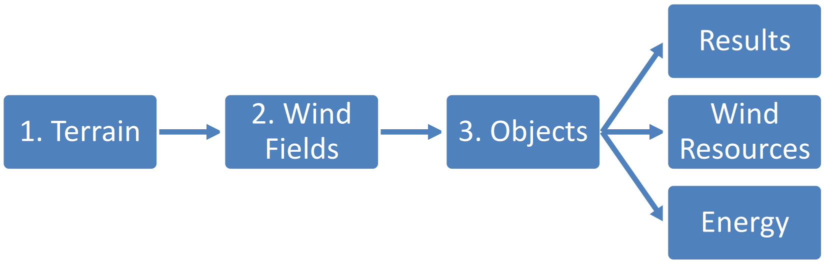

Figure 4 – Modular structure of the WindSim software. Adapted from [21].

Below a brief description of each module is provided [31]:

- **Terrain:** In this module, the three-dimensional domain of the simulation mesh is developed. The configuration of the WindSim model starts with the acquisition/conversion of the database (map format) with elevation and roughness values of the orography of the area under analysis. The spatial resolution of the terrain mesh is defined in this module.
- **Wind Field:** This module allows to obtain the "initial and boundary conditions" of the WindSim software. Based on this information is possible to correct the virtual series for the spatial points of interest. Currently, two distinct options are available for imposing these conditions: i) analytical through the defining a constant flow from a predetermined direction– the most common approach in the literature; or ii) nesting – where a forcing is imposed based on a WindSim model with low spatial resolution or on data from a mesoscale model. The application of the nesting technique allows reducing the inaccuracies introduced

by the simplifications of the analytical approach, namely, concerning the atmospheric stability at different points of the simulation domain. Additionally, in this module, it is possible to define different models of turbulence, which are central to the characterization of atmospheric flow.

- **Objects:** WindSim allows the introduction of time series in the processing of results instead of the traditional climatology file in a frequency table format, usually called “tab” file (originating format from a commercial software well-established in the wind sector – WAsP). In this module, the virtual time series are ingested to perform the spatial correction for each grid point.
- **Results:** This module allows the extraction of results in horizontal planes using the results stored in the compressed database obtained in the Wind Field module. It is even possible to visualize the extracted variables in a time-varying animation. The extraction of variables can be performed for different direction sectors according to the following options: i) absolute values of each field - normalized; ii) normalized by climatology or virtual time series data; or iii) normalized by a scalar value. The second approach is used in this work to identify the wind speed and direction correction factors.

The modules “Wind resources” and “Energy” are not used in this work. These modules are specific applications for the wind energy sectors.

One of the limitations in the WindSim is the allowed maximum number of cells to discretize the computational domain. In particular, a maximum of 1000 points for each direction is available. Therefore, the region under analysis was split into multiple grid (simulation) domains to accomplish this criterion while enabling to obtain the results with a high spatial resolution – 30 meters.

3.3 Correcting wind speed and direction

The methodology implemented in [21] requires the use of a CFD model for each forecast period. This is a time-expensive process that avoids the use in real-time. To overcome this drawback, catalogue-based correction factors (CF) for i) wind speed and ii) wind direction were implemented. The FC is scaled based on different wind direction conditions between the location of each power line segment in the CFD model and that at the virtual time series location. As commonly used in the wind sector best practices, it was decided to use twelve angular sectors with the middle points at 0^o, 30^0, 60^0… 330^0.

The catalogue uses hourly wind flow direction from the NWP model as a reference to decide the FC to be applied, as shown in Table 1.

Table 1. Example of the catalogue created for the i-*th* segments.

Power line segment number	**Wind direction sector (θ)**			
	]345º;15º]	**]15º;45º]**	**…**	**]315º;345º]**
Segment 1	$CF_{WS,1}(\theta)$; $CF_{WD,1}(\theta)$	$CF_{WS,1}(\theta)$; $CF_{WD,1}(\theta)$		$CF_{WS,1}(\theta)$; $CF_{WD,1}(\theta)$
…				
Segment *i*	$CF_{WS,i}(\theta)$; $CF_{WD,i}(\theta)$	$CF_{WS,}(\theta)$; $CF_{WD,1}(\theta)$		$CF_{WS,1}(\theta)$; $CF_{WD,1}(\theta)$

In Table 1, $CF_{WS,i}$ and $CF_{WD,i}$ correspond to the wind speed and direction correction factors, respectively. These CFs are outputs from the CFD model. Figure 5 presents the CFs for two random power line segments.

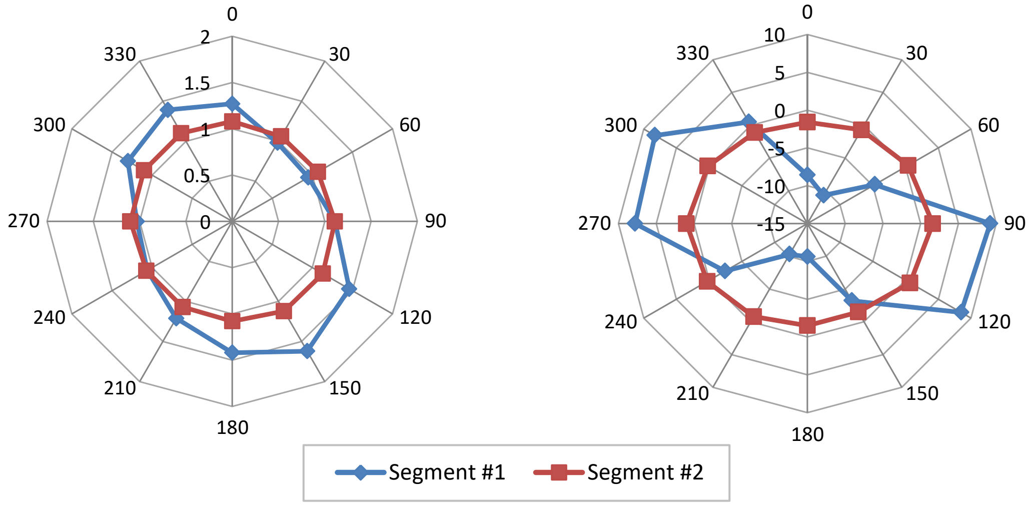

a) CF_{WS} b) CF_{WD}

Figure 5 – Correction factors for wind speed (units: dimensionless) and wind direction (unis: degree) for two random power line' segments in case study A.

During the operational phase, the wind speed - $WS\ Calibrated_i$- and direction - $WD\ Calibrated_i$ – for each segment are to be provided using the following equations:

$$WS\ Calibrated_i(t) = CF_{WS,i}(\theta) \times WS_{Mesoscale}(t,\theta) \quad (4)$$

$$WD\ Calibrated_i(t) = CF_{WD,i}(\theta) + WD_{Mesoscale}(t,\theta) \quad (5)$$

In the previous equations, $WS_{Mesoscale}(t,\theta)$ and $WD_{Mesoscale}(t,\theta)$ correspond to the wind speed and direction for the t-*th* time.

To properly describe the application of this procedure some descriptive examples are provided below using results from Figure 5. To obtain the wind speed in *Segment #1*, the correction factor that needed to be applied in the virtual time series from the mesoscale model when the wind direction is from the South sector (180º) is 1.45. For *Segment #2*, the correction in the wind speed is 1.07. In the case of the wind direction, a correction of minus 10º needs to be applied in the wind direction from the virtual time series for *Segment #1*. For segment #2, a correction of minus 1º is needed. Figure 6 provides an example of the approach implemented using the two previous lines' segment.

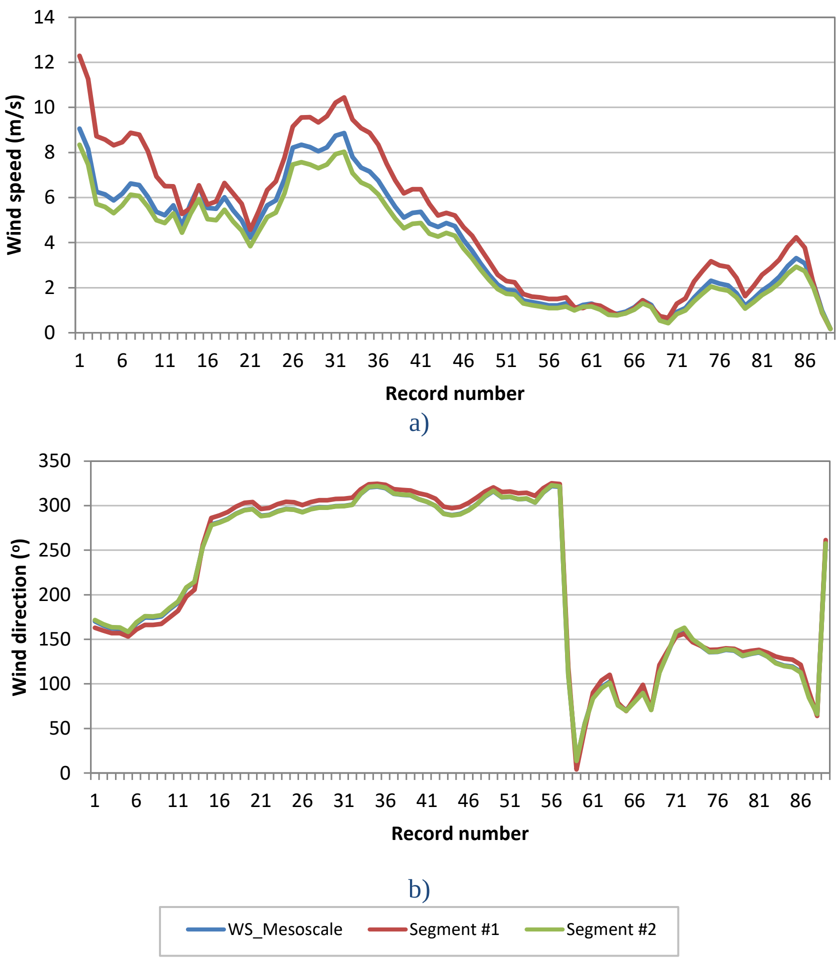

Figure 6 – Example of the correction factors application for two segments: a) wind speed; b) wind direction.

Since all interconnections overhead lines were analyzed in case study C, it was decided not to apply the CFD model. Thus, the results in this case study are based only on hourly data from the mesoscale model during 2018.

4. Results

4.1 MM5 setup

The model spatial configuration is presented in Figure 7. For the selection of this configuration the most adequate best practices were used as discussed in [32]. It was decided to use two domains with 15 km and 3 km spatial resolution, respectively with one-way coupling providing outcomes for each hour. The data were attained for 2018.

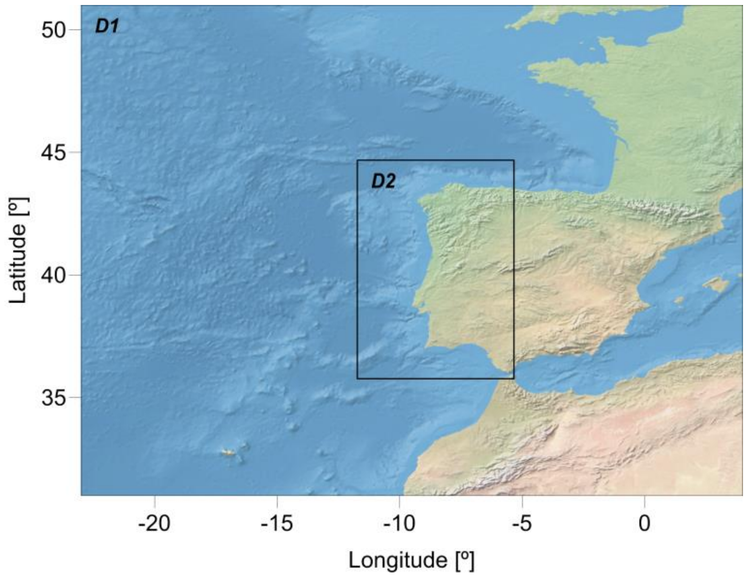

Figure 7 – MM5 geographical domains used in the OptiGRID project.

The dimensions of the grid points for each simulation domain, their spatial resolution and the model time step considered are shown in Table 2. A summary of the physical options and parameterizations used in the simulations are presented in Table 3.

Table 2. Domain dimensions and their simulation time steps.

Domain	Grid dimensions Longitude × Latitude × Altitude	Spatial resolution (km)	Model time step (s)	Forecast (h)
D1/15km	180 × 200 × 26	15	30	48h
D2/3km	171 × 291 × 26	3	6	48h

Table 3. Options and physical parameterizations considered in the MM5 model.

Domain	Data 3D	Assimilation	Cumulus parameterization	Microphysics	Atmospheric Boundary Layer	Radiation Model	Soil Model
15km	GFS 0.25	FDDA	Betts-Miller	Reisner graupel 2	MRF	Cloud-Radiation	NOAH
3km	MM5 - 15km	-	-	Reisner graupel 2	MRF	Cloud-Radiation	NOAH

4.2 NWP-CFD results

In this section, the main results for each case study are presented. The results provided are for the year 2018 (further details regarding this choice in section 5.2). Due to the dimension of the case studies A and B and the limitation of the maximum points in the CFD model several domains were created. For each subdomain, the NWP data were extracted following the most adequate procedures identified in [21] (as described in section 2.2).

In the following subsections, the average values of the correction factors and the meteorological parameters used in the DLR analysis for each power line segment are presented using figures. Based on the average values for all power line segments further statistical results are provided in a tabular format, namely, the minimum, the 5th, 25th, 50th and 75th percentiles and maximum values.

4.2.1 Case study A

Due to the dimension of case study A and the limitation of the maximum points in the CFD model, sixteen domains were established,
Figure 8.

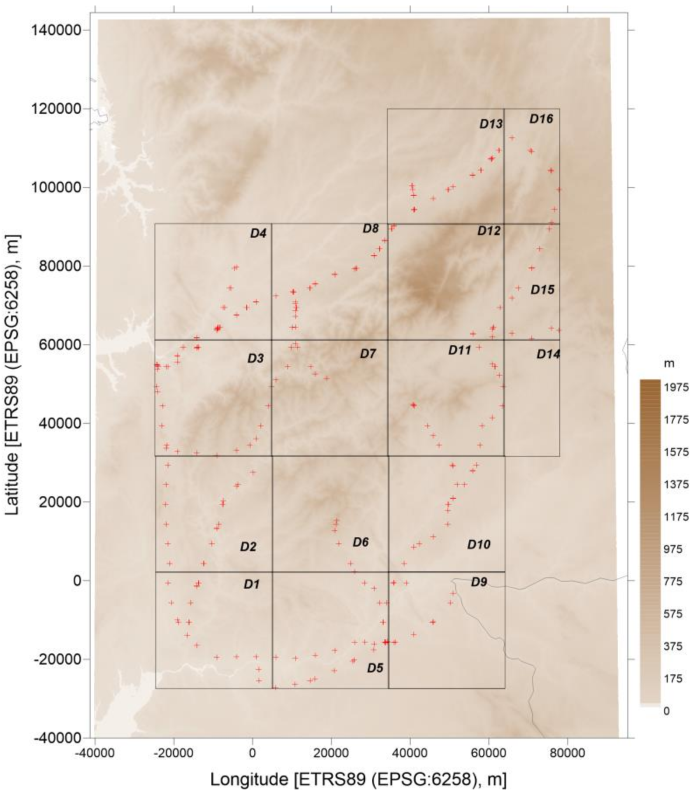

Figure 8 – WindSim geographical domains for case study A.

- Corrections factors for case study A

In Figure 9 the wind speed calibration coefficients - $CF_{WS,i}$- for the *i-th* line segments analyzed in case study A are presented. A summary of $CF_{WS,i}$ values for the North, West, South, and East directional sectors is presented in Table 4.

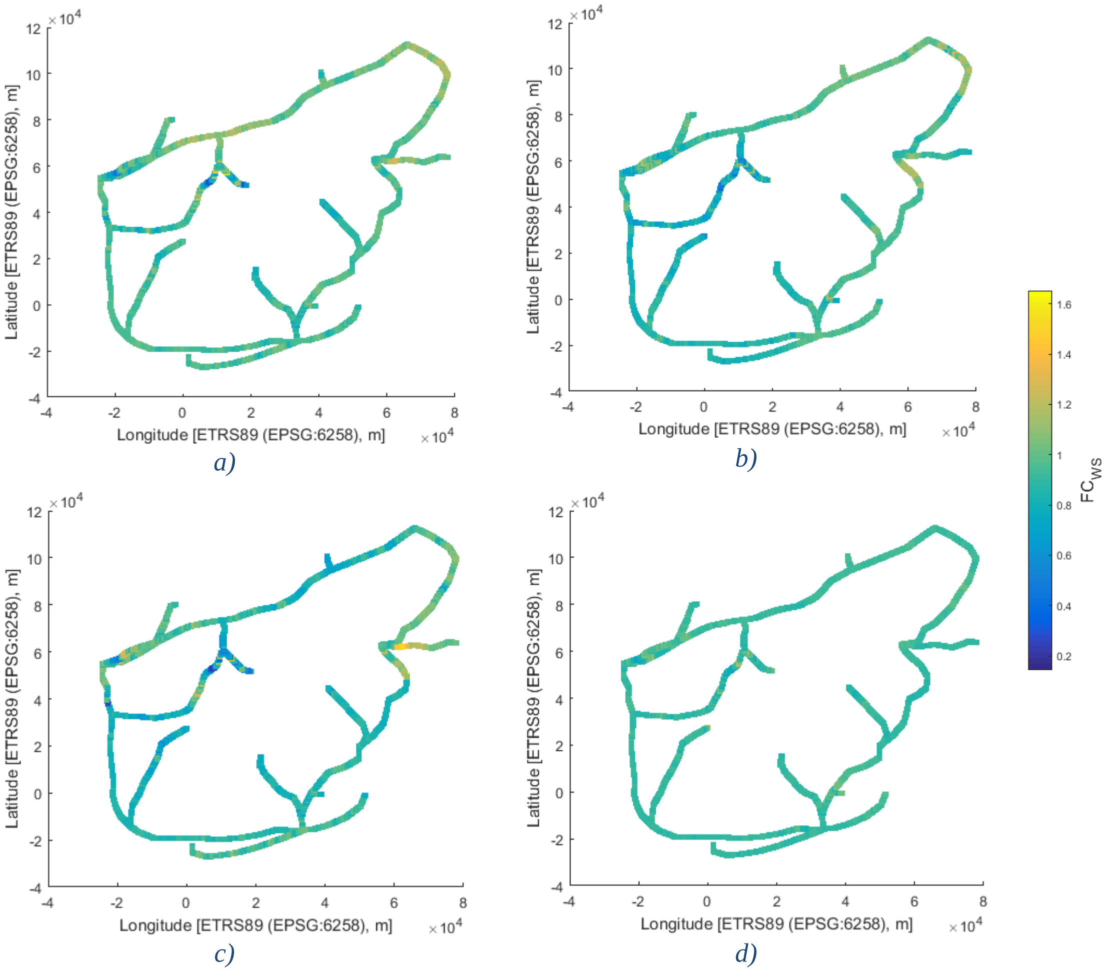

Figure 9 – $CF_{WS,i}$ for the i-th line segments in case study A using a 30 meters spatial resolution for the direction sectors: a) North; b) East; c) South and d) West.

Table 4. Summary of the main results of the CF_{WS} for case study A.

Directional sector	Minimum	Percentile					Maximum
		5	25	50	75	95	
North	0.14	0.80	0.91	0.96	1.01	1.14	1.65
East	0.34	0.71	0.84	0.92	0.97	1.09	1.37
South	0.33	0.79	0.90	0.95	1.03	1.13	1.63
West	0.27	0.72	0.84	0.90	0.98	1.10	1.36

The maximum and minimum $CF_{WS,i}$values applied to the virtual time series extracted from the mesoscale model are obtained for the North sector. The median value for the four directional sectors presented showed a value below 1, i.e., a correction factor to decrease the wind speed is applied for half of the power line's segments analyzed.

In Figure 10 the wind direction calibration coefficients - $CF_{WD,i}$- for the *i-th* line segments analyzed in case study A are presented. A summary of $CF_{WD,i}$ values for the North, West, South, and East sectors is presented in Table 5.

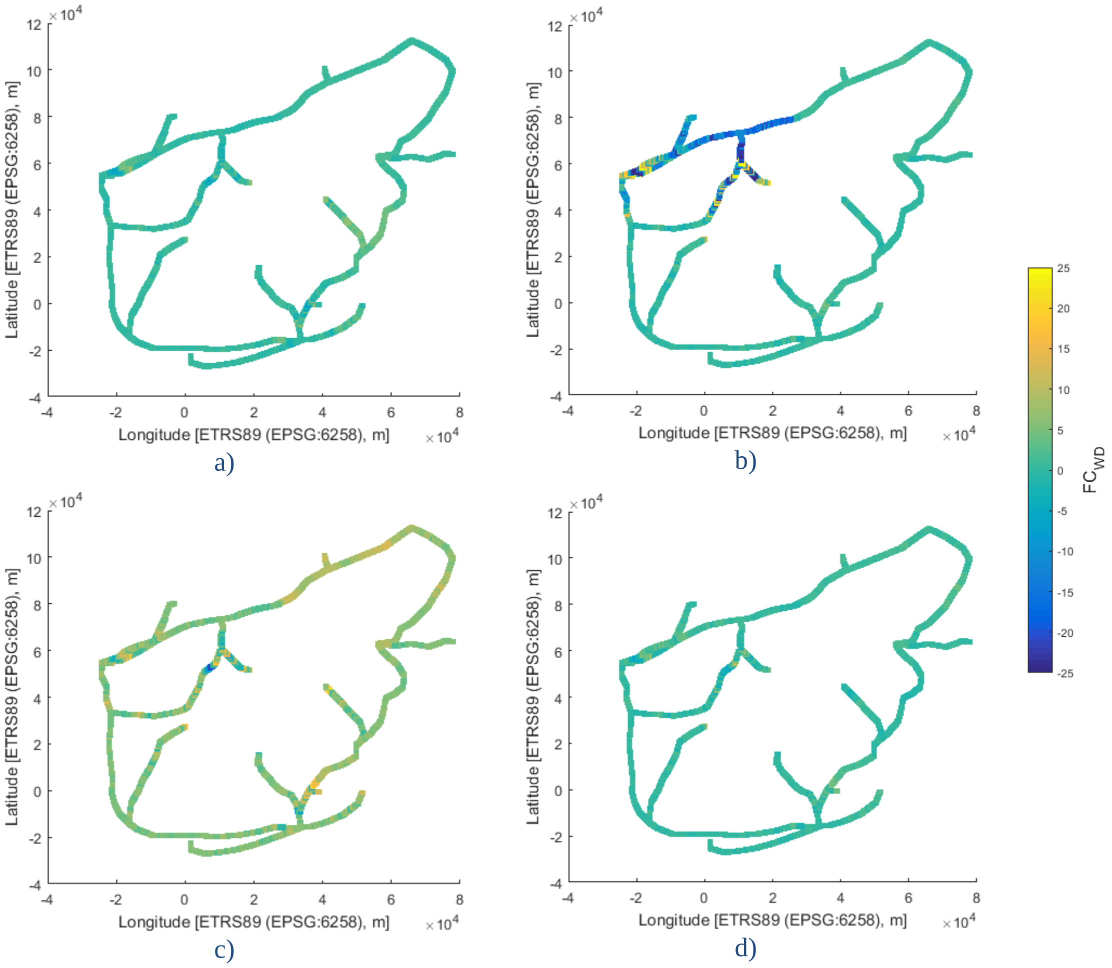

Figure 10 – $CF_{WD,i}$for the *i-th* line segments in case study A using a 30 meters spatial resolution for the direction sectors: a) North; b) East; c) South and d) West.

According to the results from Figure 10 and Table 5, the maximum and minimum $CF_{WD,i}$values applied to the virtual time series extracted from the mesoscale model are obtained for the East sector. The median value for the four directional sectors presented showed a value near of 0º. Thus, this result indicates that in half of the power line' segments no significant directional corrections are applied to the virtual time series from the MM5 model.

Table 5. Summary of the main results of the CF_{WD} for case study A.

Directional sector	Minimum	Percentile					Maximum
		5	25	50	75	95	
North	-8.66	-1.76	-0.19	0.44	1.02	3.89	11.40
East	-25.64	-17.77	-1.09	0.06	0.87	4.03	23.96
South	-12.76	-1.64	-0.32	0.30	1.01	2.31	8.37
West	-7.32	-1.60	-0.29	0.43	1.11	2.81	12.18

- Meteorological parameters for the DLR analysis for case study A

The average values of the meteorological parameters for the period simulated are depicted in Figure 11.

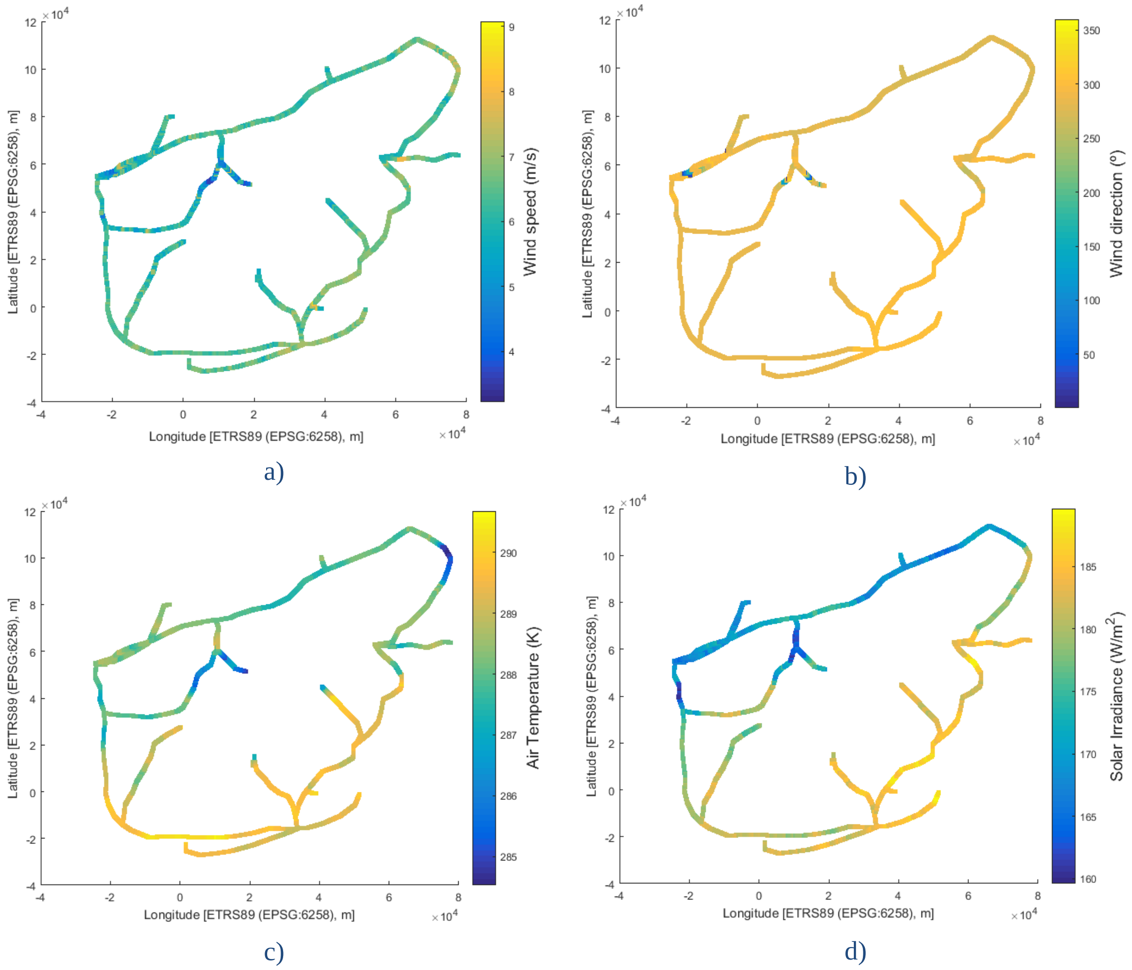

Figure 11 – Average values of the meteorological parameters used in the DLR analysis for case study A: a) wind speed, b) wind direction, c) air temperature and d) solar irradiance for each power line' segment.

Based on the average values depicted in Figure 11, a summary of the results for each meteorological parameter is provided in Table 6.

Table 6. Summary of the meteorological parameter values for case study A.

Meteorological Parameter	Minimum	Percentile					Maximum
		5	25	50	75	95	
Wind speed (m/s)	3.2	5.4	6.0	6.4	6.7	7.1	9.0
Wind direction (º)	0.3	270.7	280.0	284.9	299.2	305.8	359.9
Air temperature (K)	284.5	286.5	287.9	288.5	289.2	289.8	290.7
Solar irradiance (W/m^2)	159.6	165.6	170.4	179.2	183.1	186.3	189.6

According to the values from Figure 11 and Table 6, the yearly average wind speed observed in the power line segments can range between 3.2 to 9.0 m/s. The median value is 6.4 m/s, at 25 meters above ground level. The median average wind direction is 284.9º corresponding to a wind flow from the West/Northwest sectors. The air temperature shows a range of values of nearly 7 K from 284.5 to 290.7 K. Due to the shading effect of some mountains it is possible to observe differences in the solar irradiance of 30 W/m^2. The power line' segment with the lowest annual solar irradiance value corresponds to 159.6 W/m^2, while the segment with the highest presents a value of 189.6 W/m^2.

4.2.2 Case study B

Due to the dimension of case study B and the limitation of the maximum points in the CFD model, twenty domains were established, Figure 12.

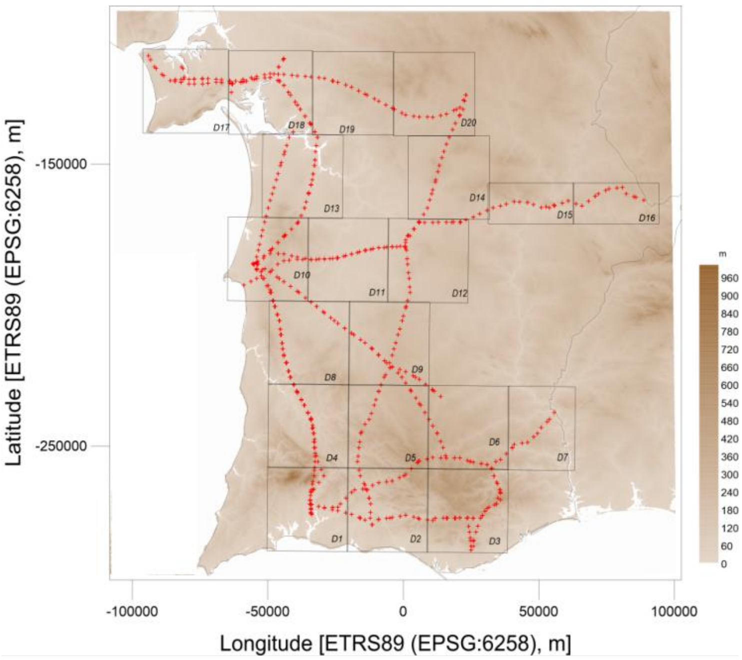

Figure 12 – WindSim geographical domains for case study B.

- Corrections factors for case study B

In Figure 13 the wind speed calibration coefficients - $CF_{WS,i}$- for the *i-th* line segments analyzed in case study B are presented. A summary of $CF_{WS,i}$ values for the North, West, South, and East sectors is presented in Table 7.

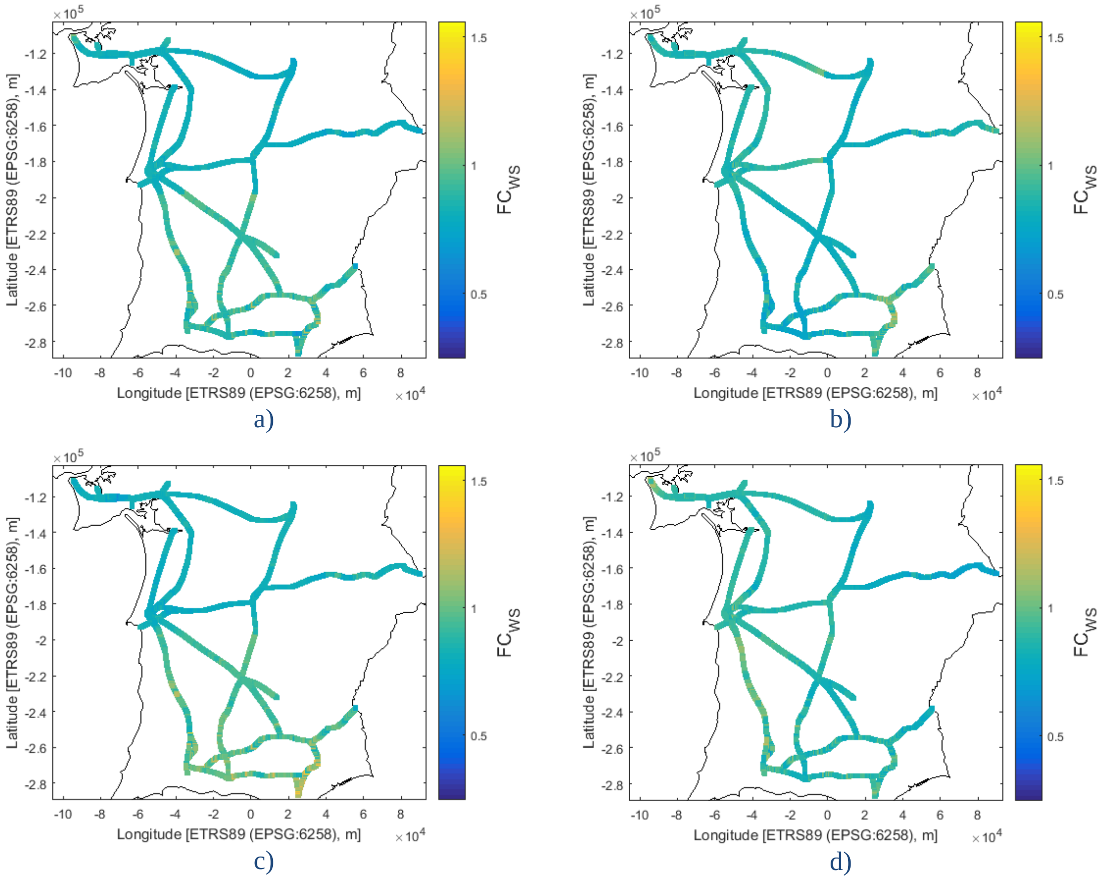

Figure 13 –$CF_{WS,i}$ for the i-th line segments in case study B using a 30 meters spatial resolution for the direction sectors: a) North; b) East; c) South and d) West.

Table 7. Summary of the CF_{WS} values for case study B.

Directional sector	Minimum	Percentile					Maximum
		5	25	50	75	95	
North	0.54	0.77	0.80	0.84	0.91	1.01	1.44
East	0.42	0.74	0.80	0.84	0.88	0.99	1.27
South	0.46	0.77	0.80	0.87	0.97	1.12	1.56
West	0.48	0.78	0.84	0.88	0.92	1.03	1.24

In Figure 14 the wind direction calibration coefficients - $CF_{WD,i}$- for the *i-th* line segments analyzed in case study B are presented. A summary of $CF_{WD,i}$ values for the North, West, South, and East sectors is presented in Table 8.

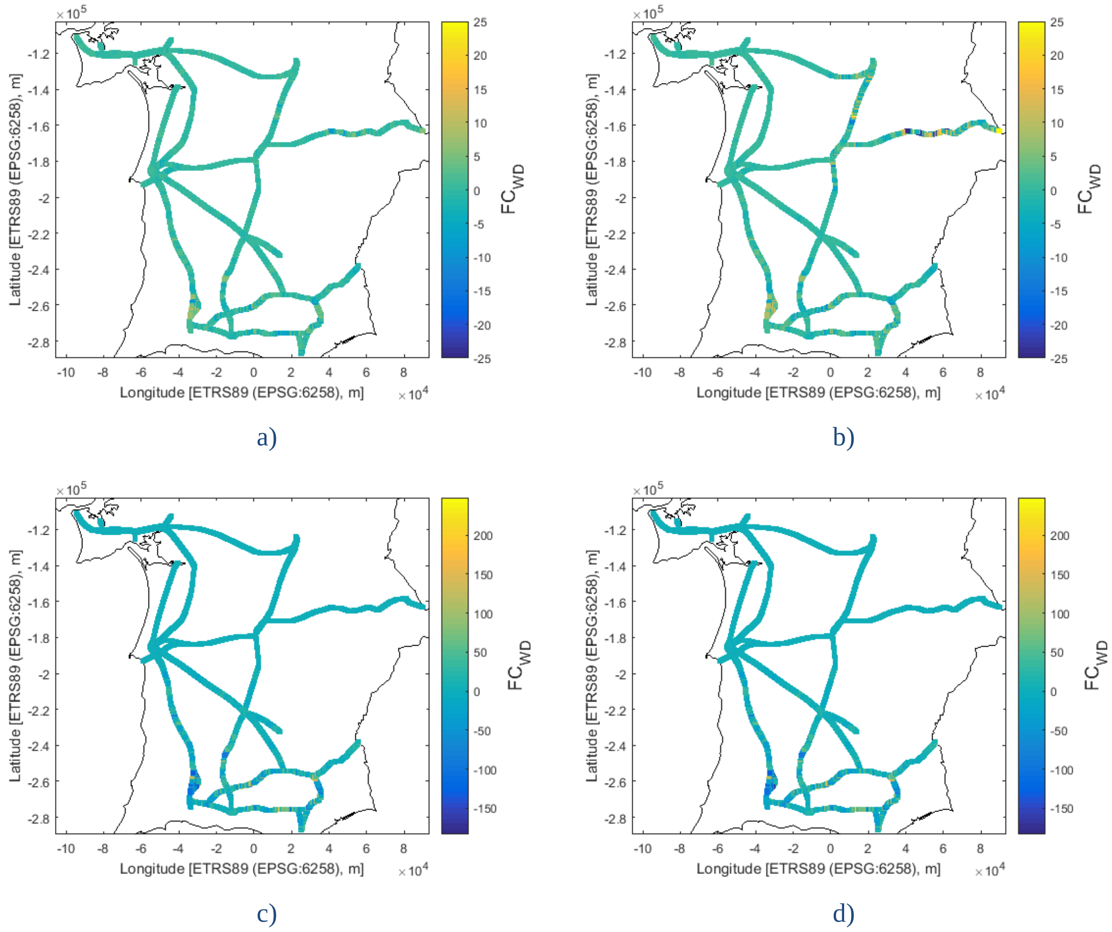

Figure 14 – $CF_{WD,i}$ for the *i-th* line segments in case study B using a 30 meters spatial resolution for the direction sectors: a) North; b) East; c) South and d) West.

Table 8. Summary of the main results of the CF_{WD} for case study B.

Directional sector	Minimum	Percentile					Maximum
		5	25	50	75	95	
North	-17.30	-3.51	-0.75	-0.01	0.66	3.08	34.38
East	-18.31	-4.24	-0.79	0.06	0.72	4.22	36.47
South	38.53	-43.65	-1.41	0.11	3.70	43.91	47.96
West	-36.87	-5.07	-0.89	0.02	0.73	4.73	56.01

- Meteorological parameters for the DLR analysis

The average values of the meteorological parameters for the period simulated are depicted in Figure 15.

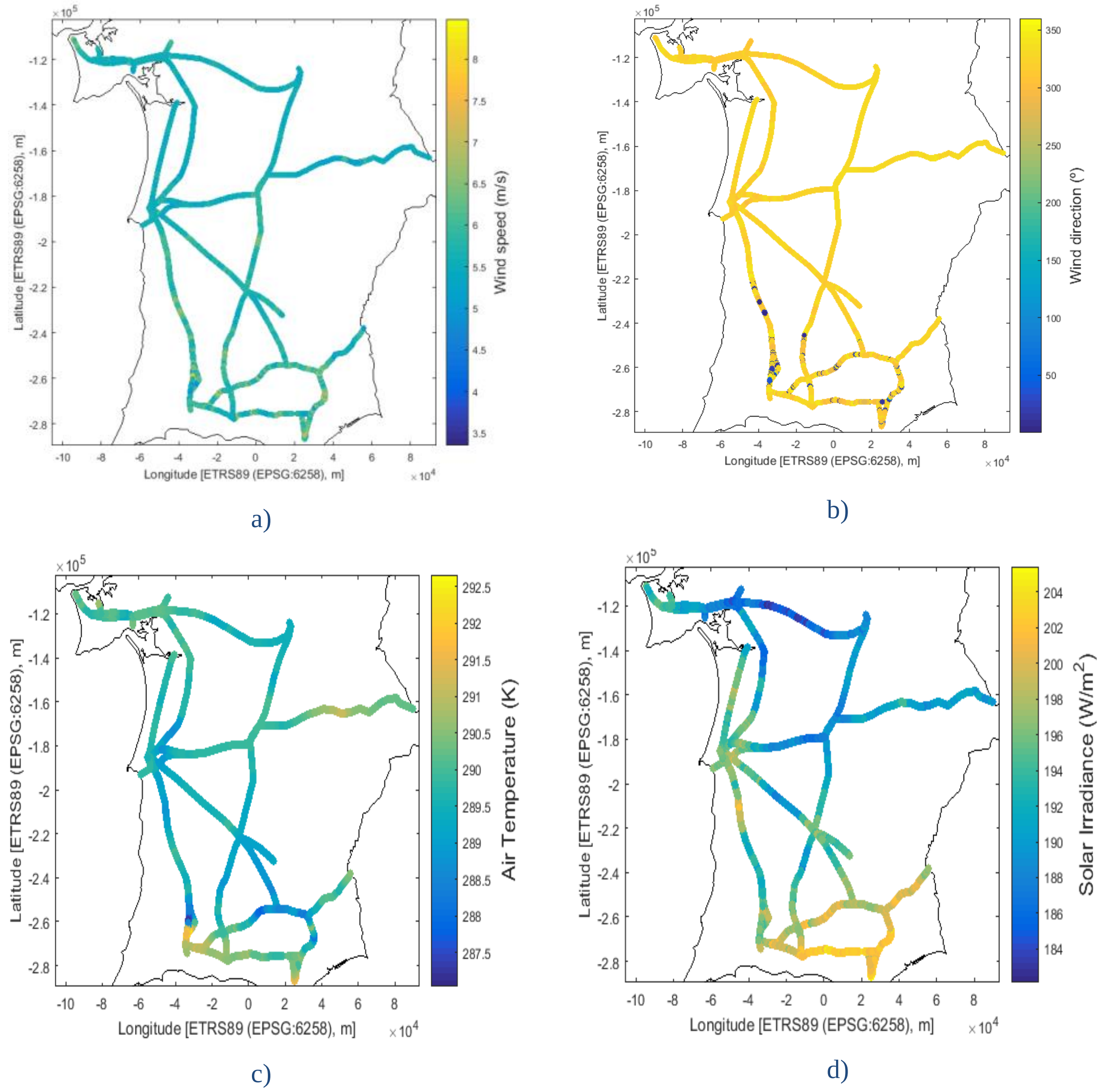

Figure 15 – Average values of the meteorological parameters used to feed the DLR analysis: a) wind speed, b) wind direction, c) air temperature and d) solar irradiance for each power line' segment of case study B.

Based on the average values depicted in Figure 15, a summary of the results for each meteorological parameter is provided in Table 9.

Table 9. Summary of the meteorological parameter values for case study B.

Meteorological Parameter	Minimum	Percentile					Maximum
		5	25	50	75	95	
Wind speed (m/s)	3.4	5.3	5.5	5.6	5.9	6.5	8.5
Wind direction (º)	0.0	286.9	314.9	324.0	331.0	342.0	359.9
Air temperature (K)	287.0	288.7	289.4	289.7	290.1	290.8	292.7
Solar irradiance (W/m^2)	182.1	186.5	190.2	194.5	198.1	202.3	205.4

According to the values from Figure 15 and Table 9, the yearly average wind speed observed in the power line segments can range between 3.4 to 8.5 m/s. The median value is 5.6 m/s, at 25 meters above ground level. The median average wind direction is 324.0º corresponding to a wind flow from the West/Northwest sectors. The air temperature shows a range of values below 6 K from 287.0 to 292.7 K. As expected, compared to case study A, the minimum and maximum air temperature values are higher in this case study B. The same occurs with the solar irradiance values. The power line' segment with the lowest annual solar irradiance value corresponds to 182.1 W/m^2, while the segment with the highest presents a value of 205.4 W/m^2.

4.2.3 Case study C

As previously indicated, in this case study, only data from the mesoscale model with 3 km are used, i.e., each power line was split into segments with 3 km spatial resolution. The average values of the meteorological parameters for the period simulated are depicted in Figure 16.

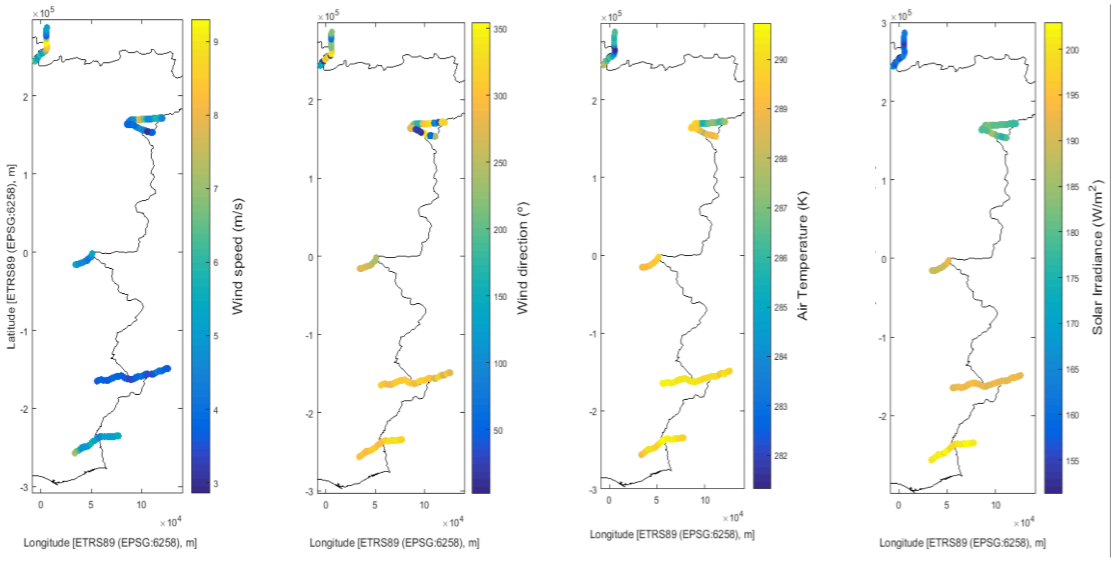

a) b) c) d)

Figure 16 – Average values of the meteorological parameters used to feed the DLR analysis: a) wind speed, b) wind direction, c) air temperature and d) solar irradiance for each power line segment of case study C.

Based on the average values depicted in Figure 16, a summary of the results for each meteorological parameter is provided in Table 10.

Table 10. Summary of the meteorological parameter values for case study C.

Meteorological Parameter	Minimum	Percentile					Maximum
		5	25	50	75	95	
Wind speed (m/s)	2.9	3.5	3.8	4.6	5.4	7.4	9.3
Wind direction (º)	137.6	146.9	169.7	186.1	207.3	243.3	253.3
Air temperature (K)	281.3	285.5	287.4	289.5	290.2	290.5	290.7
Solar irradiance (W/m^2)	151.3	158.6	178.8	185.6	192.9	201.8	202.9

According to the values from Figure 16 and Table 10, the yearly average wind speed observed in the power line segments can range between 2.9 to 9.3 m/s. The median value is 4.6 m/s, at 25 meters above ground level. The highest wind speed values are observed in the tie-lines located in the North of Portugal. The wind direction tends to show similar values for all segments in the tie-lines located in the South of Portugal. On the other hand, due to the existence of mountains and valleys, significant changes are observed in the wind speed and direction for the segments of each tie-line located in northern regions. As expected, due to the climatic conditions of Portugal, the highest air temperature and solar irradiance values are observed in the tie-lines located in the South region.

5. Merging the data needed for the DLR analysis

A final OptiGRID' dataset will be defined to cover all the regions of the network to be analyzed in each case study. Several days of operation of the Portuguese power system will be selected to highlight the added value of the DLR methodology, including under windy, sunshiny and MIBEL constraints conditions. The necessary data to conduct the OptiGRID research activities can be split into three essential types of data:

1) Portuguese transmission and distribution networks: georeferenced layout and topology of the national transmission network (identification of all buses/substations, wind, solar PV and hydropower plants) and its electrical characteristics (e.g., cables, resistance, reactance and susceptance) and the different load and generation hourly profiles. Additionally, the following information was also collected and validated: the location of the vertex towers with an indication of the busbar connections (when more than one bus/substation in the same place); the technical characteristics of transformers and the respective connecting specifications; the location, connections and technical characteristics of reactive power compensation systems (*e.g.*, shunts, and capacitor banks); and nominal loads and generation capacities associated with each busbar.

The network data gathered during this project comprises the current topology of the Portuguese transmission network (RNT), but also for future topologies of network expansion already planned by the transmission system operator (TSO) to accommodate additional levels of energy from renewable power sources. It covers the voltage levels of 400 and 220, including the interconnection with Spain. A summary of the number of wind, solar and hydropower plants in each case study as well as the number of overhead power lines and substations are presented in Table 11.

Table 11. Summary of the Portuguese transmission and distribution networks data collected.

Case study	Wind Parks	Solar PV Parks	Hydro power plants	Number of lines analysed	Number of substations
A	49	0	15	22	37
B	17	27	1	43	9
C	-	-	-	9	12

2) Historical operation of day-ahead electricity markets in MIBEL: identification of hours in which the market splitting mechanism has been activated. This comprises public information from market agents and their participation in MIBEL, including their supply and demand bids (quantity and price), as well as from MIBEL itself, namely the day-ahead and intra-day market-clearing prices, interconnection capacities, among others [34].

3) Meteorological data: The necessary meteorological data are obtained from an NWP for a time horizon encompassing the day-ahead market (DAM). To overcome the inability of this model to successfully handle sub-grid scale phenomena, *a posteriori* physical correction approach, based on computational fluid dynamics (CFD) simulation, was used to provide location-specific forecasts as dully reported in the first section of this deliverable.

The data collected and the sources were already presented in D2.1 [33], D4.1 [35] and D4.2 [36].

In addition to the previous data, the information regarding the height above ground level for each power line segment was also collected, Figure 17. This information was gathered from the NASA Shuttle Radar Topography Mission (SRTM) Version 3.0 Global 1 arc-second project[4].

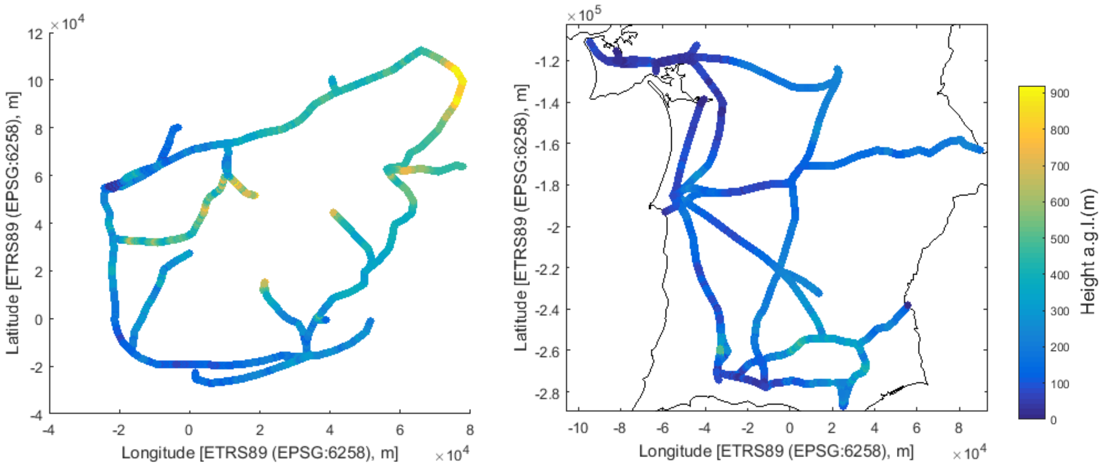

Case study A

Case study B

Figure 17 – Height above mean sea level for the power line segments for case study A and B.

[4] Available at: https://earthdata.nasa.gov/

Within the scope of this project, it was possible to obtain all the data needed to apply and validate the mathematical models under development. ,However, for disclosure reasons, only non-confidential data are presented in this report. .

5.1 Data validation applied in the OptiGRID project

The main steps of data validation implemented in OptiGRID project are depicted in Figure 18. The procedure consists of an internal peer revision with the data collecting task assigned to one person of *partner A*. Then, a second person of this partner performs a control and quality (C&Q) check of the data before sending it to partner B. *Partner B* is also responsible for carefully reviewing the data received and requesting additional information, if any problem is detected.

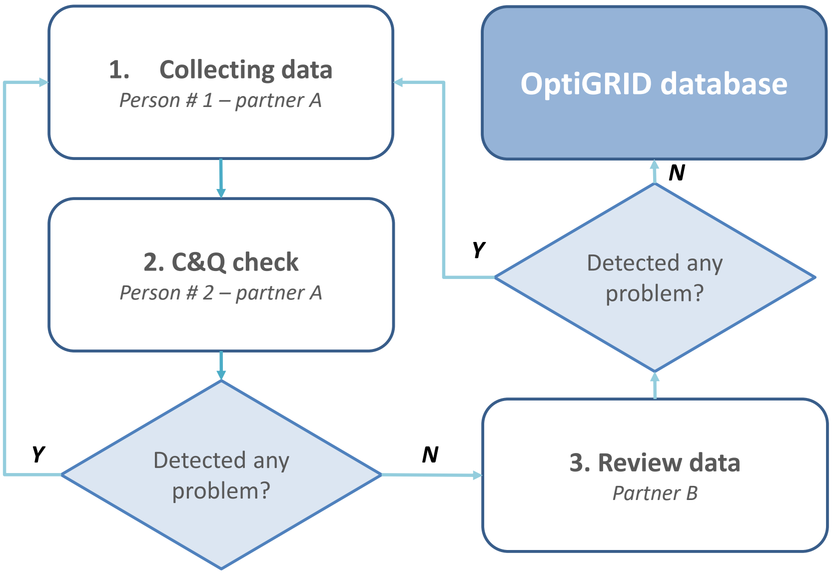

Figure 18 – Data validation procedure.

For temporal data further steps were considered using a rigorous data quality control check. This step is performed in two stages:

1. ***Automatically report*** (using in-house scripts) that performs**:**

- General system checks (number of data records and time and date of each data record);
- Measurement range tests (for each parameter and according to partners experience the range limits are defineda);

- Trends and step-change tests;
- Physical and statistical relationships between various measured parameters (e.g., correlations among power production of neighbour wind parks);
- Each suspect or invalid data is flagged and carefully analysed resorting to manual inspection.

2. ***Manually inspection*** using time series graphics that allows complementing the automatic approach to detect flaws and erroneous records. When faults, anomalies or errors are detected in the data collected, they are flagged and thorough analysis is performed using statistical-based tools. The flagged data are then validated, repeating the process of automatic inspection and/or manual. Figure 19 represents briefly this process.

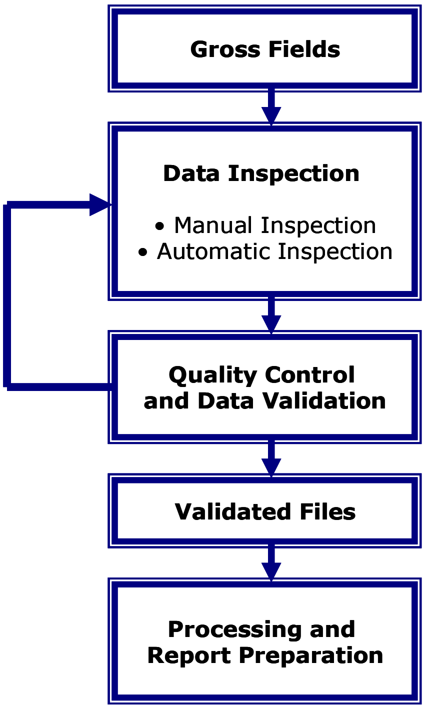

Figure 19 – Measured data C&Q control procedures.

With the application of the previous procedures, no missing or abnormal data were for now identified in the case studies under analysis.

All temporal data are in Coordinated Universal Time (UTC).

5.2 Period under analysis

As reported in D2.1, the year 2018 was used for all data collected in this project. This option corresponds to a typical meteorological year with extreme weather conditions representative of wet/dry and windy/calm periods that was selected to assess the benefits of the methodology proposed in this project. Since no substantial changes were observed in the topology and electrical characteristics of the transmission network in the case studies regions under analysis, this option also enables the use of up-to-date information regarding the transmission and distribution networks, as being representative of the situation under study.

6. Final remarks

This report describes meteorological forecast data based on a numerical weather prediction (NWP) and computational fluid dynamic (CFD) coupling approach. It also presents the main datasets and the procedures implemented to validate and merge all the data collected during the OptiGRID project.

The proposed approach was developed to focus on the real operation. In this sense, CFD catalogues-based for correction wind speed and wind direction obtained from the NWP is proposed. The catalogues use the wind direction from the NWP to decide the correction factors for each segment of the overhead power lines. Future works should comprise experimental campaigns for validation of the results obtained and to establish appropriate approaches to calibrate the air temperature and solar irradiance, which are also parameters with impact in the dynamic line analysis tool under development in this project. Based on these experimental campaigns, the coupling approach could be revised to include other relevant features of the atmospheric flow, for instance, the atmospheric stability to establish the correction factor catalogues.

Within the scope of this project, all the data needed to realize the case studies defined in Task 4 and evaluated these case studies in Task 5 were delivered/obtained.

References

[1] B. P. Bhattarai *et al.*, "Improvement of Transmission Line Ampacity Utilization by Weather-Based Dynamic Line Rating," *IEEE Trans. Power Deliv.*, vol. 33, no. 4, pp. 1853–1863, 2018, doi: 10.1109/TPWRD.2018.2798411.

[2] S. Karimi, P. Musilek, and A. M. Knight, "Dynamic thermal rating of transmission lines: A review," *Renew. Sustain. Energy Rev.*, vol. 91, no. April, pp. 600–612, 2018, doi: 10.1016/j.rser.2018.04.001. [Online]. Available: https://doi.org/10.1016/j.rser.2018.04.001

[3] E. Fernandez, I. Albizu, M. T. Bedialauneta, A. J. Mazon, and P. T. Leite, "Review of dynamic line rating systems for wind power integration," *Renew. Sustain. Energy Rev.*, vol. 53, no. 2016, pp. 80–92, Jan. 2016, doi: 10.1016/j.rser.2015.07.149. [Online]. Available: http://dx.doi.org/10.1016/j.rser.2015.07.149

[4] A. Couto, L. Rodrigues, P. Costa, J. Silva, and A. Estanqueiro, "Wind power participation in electricity markets - The role of wind power forecasts," in *EEEIC 2016 - International Conference on Environment and Electrical Engineering*, 2016, p. 6, doi: 10.1109/EEEIC.2016.7555453.

[5] R. Marujo, P. Costa, M. Fernandes, T. Simoes, and A. Estanqueiro, "Offshore wind field: Application of statistical models as a spatial validation technique," in *European Offshore Wind Conference & Exhibition*, 2011, p. 8 [Online]. Available: https://repositorio.lneg.pt/bitstream/10400.9/1501/1/EWEA_Amsterdam_RMarujo_ PCosta_MFernandes_AEstanqueiro.pdf

[6] J. Silva, F. Marques da Silva, A. Couto, and A. Estanqueiro, "A method to correct the flow distortion of offshore wind data using CFD simulation and experimental wind tunnel tests," *J. Wind Eng. Ind. Aerodyn.*, vol. 140, 2015, doi: 10.1016/j.jweia.2015.01.017.

[7] R. E. Keck and N. Sondell, "Validation of uncertainty reduction by using multiple transfer locations for WRF-CFD coupling in numerical wind energy assessments," *Wind Energy Sci.*, vol. 5, no. 3, pp. 997–1005, 2020, doi: 10.5194/wes-5-997-2020.

[8] C. Meissner and D. Weir, "Utilizing WRF data in CFD models for wind energy assessment," in *EWEA*, 2011, p. 154.

[9] J. Duque, D. Santos, A. Couto, and A. Estanqueiro, "Optimal management of power networks using a dynamic line rating approach," *Renew. Energy Power Qual. J.*, vol. 1, no. 16, pp. 584–589, Apr. 2018, doi: 10.24084/repqj16.398. [Online]. Available: http://www.icrepq.com/icrepq18/398-18-duque.pdf

[10] D. L. Alvarez, F. F. da Silva, E. E. Mombello, C. L. Bak, and J. A. Rosero, "Conductor temperature estimation and prediction at thermal transient state in dynamic line rating application," *IEEE Trans. Power Deliv.*, vol. 33, no. 5, pp. 2236–2245, Oct. 2018, doi: 10.1109/TPWRD.2018.2831080.

[11] D. M. Greenwood, "Quantifying the benefits and risks of real-time thermal ratings in electrical networks," Newcastle University, 2014.

[12] A. W. Abboud *et al.*, "Coupling computational fluid dynamics with the high resolution rapid refresh model for forecasting dynamic line ratings," *Electr. Power Syst. Res.*, vol. 170, no. February, pp. 326–337, 2019, doi: 10.1016/j.epsr.2019.01.035. [Online]. Available:

https://doi.org/10.1016/j.epsr.2019.01.035

[13] A. Michiorri *et al.*, “Forecasting for dynamic line rating,” *Renew. Sustain. Energy Rev.*, vol. 52, pp. 1713–1730, Dec. 2015, doi: 10.1016/j.rser.2015.07.134. [Online]. Available: https://linkinghub.elsevier.com/retrieve/pii/S1364032115007819

[14] J. Iglesias *et al.*, “Guide for thermal rating calculations of overhead lines,” *CIGRÉ WG B2.43*, p. 93, 2014 [Online]. Available: http://hdl.handle.net/2268/178855

[15] E. Fernandez, I. Albizu, M. T. Bedialauneta, A. J. Mazon, and P. T. Leite, “Review of dynamic line rating systems for wind power integration,” *Renew. Sustain. Energy Rev.*, vol. 53, pp. 80–92, 2016, doi: 10.1016/j.rser.2015.07.149.

[16] J. Standen, C. Wilson, S. Vosper, and P. Clark, “Prediction of local wind climatology from Met Office models: Virtual Met Mast techniques,” *Wind Energy*, vol. 20, no. 3, pp. 411–430, Mar. 2017, doi: 10.1002/we.2013. [Online]. Available: https://onlinelibrary.wiley.com/doi/10.1002/we.2013

[17] J. M. L. M. Palma, F. A. Castro, L. F. Ribeiro, A. H. Rodrigues, and A. P. Pinto, “Linear and nonlinear models in wind resource assessment and wind turbine micro-siting in complex terrain,” *J. Wind Eng. Ind. Aerodyn.*, vol. 96, no. 12, pp. 2308–2326, 2008, doi: 10.1016/j.jweia.2008.03.012.

[18] C. G. Nunalee, C. Meißner, A. Vignaroli, N. Carolina, and R. Nc, “Downscaling MERRA mesoscale data for the generation microscale wind fields using CFD,” in *Spain: Europe's Premier Wind Energy Event*, 2014, p. 1.

[19] C. Schmitt, C. Meissner, and D. Weir, “Influence Of Thermal Stratification on CFD Simulations,” *Europe's Premier Wind Energy Event poster*. EWEA, Brussels, p. 1, 2011 [Online]. Available: https://windsim.com/Windsimarchive/library -- papers-presentations/Influence Of Thermal Stratification on CFD Simulations.pdf

[20] A. Couto, J. Silva, P. Costa, D. Santos, T. Simões, and A. Estanqueiro, “Towards a high-resolution offshore wind Atlas - The Portuguese Case,” *J. Phys. Conf. Ser.*, vol. 1356, p. 012029, Oct. 2019, doi: 10.1088/1742-6596/1356/1/012029. [Online]. Available: https://iopscience.iop.org/article/10.1088/1742-6596/1356/1/012029

[21] F. Melo, “Acoplamento modelos mesoescala / microescala - calibração para aplicações de análise dinâmica da capacidade de transmissão de linhas eléctricas Agradecimentos,” 2020 [Online]. Available: https://repositorio.ul.pt/bitstream/10451/45457/1/ulfc125990_tm_Frederico_Melo.pdf

[22] G. Grell, J. Dudhia, and D. R. Stauffer, “A description of the Fifth-Generation Penn State/NCAR Mesoscale Model (MM5),” 1995 [Online]. Available: http://nldr.library.ucar.edu/collections/technotes/asset-000-000-000-214.pdf

[23] A. Couto, J. Silva, P. Costa, D. Santos, T. Simões, and A. Estanqueiro, “Towards a high-resolution offshore wind Atlas - The Portuguese Case,” *IOP Conf. Ser. J. Phys. Conf. Ser.*, vol. 1356, no. 012029, p. 14, Oct. 2019, doi: 10.1088/1742-6596/1356/1/012029.

[24] U. S. D. of C. National Centers for Environmental Prediction, National Weather Service, NOAA, “NCEP GFS 0.25 Degree Global Forecast Grids Historical Archive.” Research Data Archive at the National Center for Atmospheric Research, Computational and Information Systems Laboratory, Boulder CO, 2015 [Online]. Available: https://doi.org/10.5065/D65D8PWK

[25] A. Couto, P. Costa, J. Silva, D. Santos, T. Simões, and A. Estanqueiro, "Planeamento das energias renováveis offshore em Portugal: D2.2 - Validação do potencial energético offshore," 2019 [Online]. Available: http://offshoreplan.lneg.pt/wp-content/uploads/2020/06/D2.2-Validacao-potencial-energetico-offshore.pdf

[26] M. Bilal, Y. Birkelund, M. Homola, and M. S. Virk, "Wind over complex terrain – Microscale modelling with two types of mesoscale winds at Nygårdsfjell," *Renew. Energy*, vol. 99, pp. 647–653, Dec. 2016, doi: 10.1016/j.renene.2016.07.042.

[27] C. Meissner, A. R. Gravdahl, and B. Steensen, "Including thermal effects in CFD simulations," in *European Wind Energy Conference and Exhibition*, 2009, p. 1.

[28] P. Theodoropoulos and N. Deligiorgis, "Windsim cfd model validation in a mixed coastal and mountainous region with complex terrain," *Lab. Istos Renewables*, pp. 1–11, 2009.

[29] Y. Liu *et al.*, "Evaluation of the wind resource for a coastal site in Mexico by combining WindSim with WRF," *J. Wind Eng. Ind. Aerodyn.*, vol. 99, no. 4, pp. 308–319, Apr. 2011, doi: 10.1016/j.jweia.2011.01.013.

[30] T. Wallbank, "WindSim validations study - CFD validation in complex terrain," WindSim AS., 2008.

[31] C. Meissner, "WindSim Getting Started 7," WindSim, 2015.

[32] T. T. Warner, "Quality assurance in atmospheric modeling," *Am. Meteorol. Soc.*, vol. 92, no. 12, pp. 1601–1610, 2011, doi: 10.1175/BAMS-D-10-00054.1.

[33] A. Couto and H. Algarvio, "D2.1 - Validation of transmission network and MIBEL data," *OptiGRID technical report*. p. 25, 2020.

[34] REN, "Energy Markets Information System," 2020. [Online]. Available: www.mercado.ren.pt. [Accessed: 01-Aug-2020]

[35] R. Pestana, C. Yang, and A. Couto, "D4.1 - Development of RES Case studies A and B: regions predominantly with a) wind distributed generation and b) with photovoltaic distributed generation," *OptiGRID technical report*. p. 47, 2020.

[36] C. Yang, J. Esteves, and R. Pestana, "D4.2 - Development of Case Study C - Market splitting scenarios in MIBEL," *OptiGRID technical report*. p. 43, 2021.

Annex A

Conductor and ambient characteristics used in Figure 1

Table A.1 shows the conductor characteristic values assumed to obtain the results presented in Figure 1. The values are the ones used in “Example B” in “CIGRÉ – Annex E Examples of calculation”, which corresponds to “Drake” 26/7 ACSR conductor at a temperature of 100ºC.

Table A. 1 Conductor characteristics considered in Figure 1.

Conductor characteristics	Values
Conductor outside diameter (mm)	28.1
Core diameter (mm)	10.4
Outer strand diameter (mm)	4.44
Maximum allowable conductor temp. (°C)	100
Emissivity	0.9
Solar absorptivity	0.9
Conductor ac resistance at 25°C (Ω/m)	7.283E-05
Conductor ac resistance at 75°C (Ω/m)	8.688E-05

Table A.2 shows the values range used in the sensitivity tests to obtain the results presented in Figure 1. The fixed values were randomly imposed for the purposes of illustration.

Table A. 2 Ambient characteristics considered in Figure 1.

Parameter	Fixed values	Values range in the sensitivity tests
Ambient air temperature (ºC)	15	[0, 10, 15, …, 35, 40]
Wind speed (m/s)	5	[1, 2, …19, 20]
Wind angle attack (º)	45	[5, 15, …, 85, 90]
Solar irradiance (W/m^2)	500	[0, 100, …, 1200, 1300]
Height above sea level (m)	500	-